7. DYNAMIC SIMULATION OF BUBBLY FLOW IN BUBBLE COLUMN BY EULERIAN/EULERIAN METHOD

7.1. Introduction

Bubble column reactors are widely used in chemical industry due to their excellent heat transfer characteristics and simple construction. The fundamental properties of the hydrodynamics in bubble columns, which are essential for scale-up and design, are still not fully understood at the current stage mainly due to the complicated nature of multiphase flow. Based on the experimental evidence, for example, the works by Tzeng *et al*. (1993) and Devanathan *et al*. (1995), it is clear that, beside the time-averaged quantities, the transient behavior of flow is required to provide further information on the fluid dynamics and transport parameters in such reactors. For instance, to study the mixing process and develop the axial dispersion models which are commonly adopted in the design and evaluation of bubble column performance, one needs the time-dependent velocity field for calculating the convection and turbulent dispersion of the passive scalar in the liquid and/or gas phase. Currently, the experimental techniques for multiphase flow include the computer-automated radioactive particle tracking (CARPT) and the particle image velocimetry (PIV). The former is a Lagrangian measurement. Devanathan *et al*. (1990) and Yang *et al*. (1995) have employed this technique to investigate the liquid velocity field in cylindrical bubble columns. The PIV system, originally developed for the velocity measurement in single-phase flow, has recently been used for multiphase systems at low volume fraction of the dispersed phase. One of the advantages of PIV technique is its capability of providing the instantaneous velocity field in the place of investigation. This type of measurement for the gas-liquid flow in bubble columns has been realized by Chen and Fan (1992) and Chen *et al*. (1994). With the rapid development of computational fluid dynamics (CFD) and increase in the computing power, the numerical simulation of multiphase flow is being recognized as a potential primary tool for the investigating and thus improving the performance of various multiphase contactors like bubble columns.

Two-phase bubbly flow is commonly defined as a flow pattern in which the gas phase is distributed within a liquid continuum in discretized bubbles much smaller than the characteristic dimension of the container (e.g. column diameter). Numerical simulation of two-phase flows either treats the system in an averaged sense as interpenetrating continuum, or explicitly moves bubbles due to the fluid-imposed and body forces---in some cases feeding back the effect of the bubbles on the carrier-fluid motion through various means. The first type of approach is called Eulerian/Eulerian method, while the second is usually referred to as Eulerian/Lagrangian method. In the first the two-fluid model is developed to describe the motion for each of the two phases in Eulerian frame of reference. In the second approach, while the continuous phase is still described in the Eulerian representation, the dispersed phase is instead treated as it is, i.e. the discrete bubbles, and each bubble is tracked by solving its equation of motion through the continuous phase. Both approaches have their own advantages and disadvantages and are commonly employed in fundamental research and engineering applications. A review on the state of art of the modeling of gas-liquid flow in bubble columns and loop reactors can be found in Sokolichin and Eigenberger (1994).

During the last several years the dynamic simulation of gas-liquid flow in bubble column reactors has drawn a considerable attention of the investigators in chemical reaction engineering community. Webb *et al*.(1992) and Lapin and Lubbert (1994) studied the gas-liquid flows in two-dimensional bubble columns. They used a single-fluid model in which the two-phase flow is regarded as a quasi-single-phase flow with variable density. Bubbles are considered to individually rise in this fluid flow, thus, leading to a dynamical change of its density which finally results in a convective flow of the bubble/liquid two-phase system. The gas phase motion is calculated by either solving the bubble distribution density function or individually tracking the bubbles or bubble clusters in a Lagrangian frame. The liquid circulation pattern in the columns of low aspect ratio has been observed in their simulation. Using an Eulerian/Eulerian model, Sokolichin and Eigenberger (1994) presented a laminar, dynamic two-dimensional simulation of gas-liquid bubble flow in a flat and uniformly aerated bubble column. In their study, no turbulence model was used in solving the velocity filed of the liquid phase and the drag force was calculated with a constant drag coefficient which leads to a mean bubble slip velocity of about 20 cm/s for air bubbles of 1-10 mm mean diameter in water. Their results are further compared with the laboratory observations and data in a flat bubble column and a loop reactor by Becker *et al*. (1994). The experimental techniques employed were Laser Doppler anemometer (LDA) for liquid velocity, a fiber optical probe for bubble velocity and an electroconductivity probe for gas holdup. The experiments and simulations were conducted in a partially aerated bubble column operating at low superficial gas velocities (about 0.3-0.6 cm/s) and in an airlift loop reactor. They showed good qualitative agreement of the numerical results and data for both the steady state and the transient behavior. By simply increasing the liquid's molecular viscosity by a factor of 100 to account for the influence of turbulence viscosity, they found a good quantitative agreement as well. However the quantitative comparisons presented in the paper are very limited (In fact, only a number of gas holdup profiles in an airlift loop reactor are shown.).

In a series of papers, Delnoij *et al*. (1997; 1997a; 1997b) numerically investigated the gas-liquid flow in two-dimensional bubble columns by Eulerian/Lagrangian methods. The motion of gas phase was solved by applying either discrete bubble model or volume of fluid (VOF) model. Unlike the work by Lapin and Lubbert (1994) where the coupling between the gas and liquid phase was achieved through the effective density of the mixture and no momentum exchange was incorporated, Delnoij *et al*. (1997) coupled the two phases by adding a source term, which includes all the forces imposed on the liquid surrounding the bubbles, into the volume-averaged Navier-Stokes equation of the liquid phase. The gas phase was described by the equations of motion for each individual bubble. In order to prevent bubble-bubble overlap during the simulation, a collision model was also developed for direct bubble-bubble interaction. Again, no turbulence model was used in the simulation. The authors compared the results, mostly in a qualitative way, with the experiment on a partially aerated quasi-two-dimensional bubble column by Becker *et al*. (1994) and studied the effect of column aspect ratio on the flow structure.

In the field of numerical study on multiphase hydrodynamics of bubble columns, considerable efforts have been devoted to the Eulerian/Lagrangian type of simulations, mostly two-dimensional, in the recent year due to, may be, the tremendous growth in computing power. It is also well understood that the Eulerian/Lagrangian method is more suitable for fundamental

investigations since it allows for a direct consideration of various effects related to bubble-bubble and bubble-liquid interaction. Instead, for practical applications, in which the high gas superficial velocity results in high gas holdup and turbulence or even churn turbulence, Eulerian/Eulerian method is usually preferred. However, several challenging issues regarding to the modeling of averaged equations and closure relations, which have been the active research topic in the field of multiphase flow for many years, still exist. One of these issues is how to model the inter-phase momentum exchange which is related to the problem of calculating the force acting on the bubble and taking into account the effect of multi-bubble (or finite value of gas holdup) on these forces. Another unresolved issue is the modeling of turbulence in two-phase flow.

It is noted that the previous studies compared the numerical predictions with the experimental measurement mostly in a qualitative way while only a few, if any, quantitative comparisons were made. Therefore, although the qualitative comparisons are satisfactory in general, limited conclusion regarding the validation and reliability of the numerical prediction can be drawn from these studies. This is, perhaps, partially due to the difficulties in getting the reliable measurement for multiphase system. Recently Lin *et al*. (1996) and Mudde *et al.* (1997) presented their experimental studies on two-dimensional bubble column at low gas volume fraction by using the PIV technique. They provided the detailed measurement of liquid velocity and turbulence intensities for the columns of different sizes and under different operating conditions. They also studied the characteristics of the macroscopic flow structures, i.e. the central meandering plume and the companion vortical regions, by measuring their frequency, wave-length and moving speed. This information provided a better understanding of gas-liquid flow in a 2-D bubble column and generated a database for the further investigations.

In the present study we present an Eulerian/Eulerian dynamic simulation of two dimensional gas-liquid bubble column. The ensemble-averaged equations are used to solve the velocity and volume fraction field for both phases. A model of bubble-induced turbulent viscosity is incorporated into the momentum equations for the liquid phase. The effect of the gas volume fraction on the inter-phase momentum exchange term is also included. The numerical predictions of macroscopic structures and mean properties are compared with the experimental data provided by Mudde *et al*. (1997) and Lin *et al*. (1996). By these comparisons, we verify that the dynamic simulation of Eulerian/Eulerian type is able to capture the flow structure in a 2-D bubble column and provide a satisfactory quantitative results for the cases which are within the bubbly flow regime.

7.2 Ensemble Averaged Equations for Two-Phase Flow

Many attempts have been made to derive the averaged equations for disperse two-phase flows (see, e.g. Drew 1983; Wallis 1991: Zhang and Prosperetti (1997). Either the volume averaging or the ensemble averaging technique can be used to derive the equations of so-called 'two-fluid' form widely used in engineering. In the recent ensemble averaging approach present by Zhang and Prosperetti (1997), the exact Navier-Stokes equations for the continuous phase is averaged by using the phase ensemble averaging method (i.e. averaged over all the configurations such that at time t the position $\mathbf{x}$ is occupied by the continuous phase). For the

disperse phase a method of 'particle' ensemble average is introduced, in which global particle attributes (e.g. the velocity of the center of mass) are averaged directly. In other word the averaged equations for the dispersed phase are obtained by directly ensemble averaging the equation of motion of particles where each particle is treated as a single identity.

For the incompressible liquid and gas the continuity equations for each phase are written as

$$\frac{\partial \epsilon_c}{\partial t} + \nabla.(\epsilon_c \mathbf{u}_c) = 0 \tag{1}$$

and

$$\frac{\partial \epsilon_d}{\partial t} + \nabla.(\epsilon_d \mathbf{u}_d) = 0 \tag{2}$$

The momentum equation for the liquid phase is written as

$$\rho_c \epsilon_c \left(\frac{\partial \mathbf{u}_c}{\partial t} + \mathbf{u}_c.\nabla \mathbf{u}_c \right) = \rho_c \epsilon_c \mathbf{g} - \epsilon_c \nabla p - (\mathbf{M}_d + \mathbf{M}_{vm}) + \nabla.(\epsilon_c \sigma_c) + \nabla.(\epsilon_c \sigma_c^b) \tag{3}$$

where the stress tensor, τ_c, is related with the velocity field by

$$\sigma_c = \mu_c^* (\nabla \mathbf{u}_c + \nabla \mathbf{u}_c^T) \tag{4}$$

where μ_c^* is the well-known effective viscosity of a dilute suspension of particles (see, e.g. Batchelor (1967))

$$\frac{\mu_c^*}{\mu_c} = 1 + \frac{5}{2}\epsilon_d + O(\epsilon_d) \tag{5}$$

The inter-phase momentum exchange terms describing the drag force M_d, and added mass force M_{vm}, are defined as

$$\mathbf{M}_d = \frac{6\epsilon_c \epsilon_d}{\pi d_p^3} \mathbf{F}_d \tag{6}$$

and

$$\mathbf{M}_{vm} = \frac{1}{2}\epsilon_c \epsilon_d C_{vm} \left(\frac{D\mathbf{u}_c}{Dt} - \frac{D\mathbf{u}_d}{Dt} \right) \tag{7}$$

where $\frac{D}{Dt}$ represents the substantial derivative.

As derived by Zhang and Prosperetti (1997), the momentum equation for the gas phase can be obtained by ensemble averaging the equation of motion of a spherical bubble moving through fluid, which gives,

$$\rho_d \varepsilon_d \left(\frac{\partial \mathbf{u}_d}{\partial t} + \mathbf{u}_d . \nabla \mathbf{u}_d \right) = \rho_d \varepsilon_d \mathbf{g} - \varepsilon_d \nabla p + \left(\mathbf{M}_d + \mathbf{M}_{vm} \right) \tag{8}$$

Since each bubble moves as a whole object, the rotational and the internal motion of the bubbles are neglected. As a result a term related to the shear stress of the gas phase vanishes. Equation 8 explicitly indicates that the bubbles respond to the continuous-phase pressure, rather than to some dispersed-phase pressure. This feature is in agreement with physical intuition. The dispersed-phase press, i.e. the pressure inside the bubble, cannot affect the motion of the bubbles directly, but only indirectly through its relation with the continuous-phase pressure resulting from dynamic boundary conditions at the bubble surface. In the present situation there is no need to solve the momentum equation for the gas, but only to state that the gas pressure is spatially uniform inside each bubble.

For quantitative analysis, it is necessary not only to derive the correct form of these equations but also to obtain reliable estimates of the various averaged quantities, such as the viscous drag and added mass coefficients that appear in the averaged equations. As is well known, the drag force acting on a spherical object moving at u_d through a fluid with velocity u_c can be expressed as

$$\mathbf{F}_d = \frac{1}{8} \rho_c \pi d_p^2 C_D \left| \mathbf{u}_c - \mathbf{u}_d \right| \left(\mathbf{u}_c - \mathbf{u}_d \right) \tag{9}$$

The drag coefficient C_D depends on the flow regime and the liquid properties. As a classical problem, the drag coefficient of a gas bubble in liquid has been extensively studied through the years. A widely used reference is Clift *et al*. (1978). Here we used the recent results by Tsuchiya *et al.* (1997). The drag coefficient of a bubble in a sufficiently contaminated system can be expressed by

$$C_D = \max\left[\frac{24}{\mathrm{Re}} \left(1 + 0.15\,\mathrm{Re}^{0.687} \right),\ f\,\frac{8}{3}\frac{Eo}{Eo+4} \right] \tag{10}$$

where the Eotvos number, Eo, is defined as

$$Eo \equiv g \rho_c d_p^2 / \sigma \tag{11}$$

The bubble Reynolds number, *Re*, is based on the bubble diameter d_p, liquid viscosity μ and the relative velocity between phase, i.e. the slip velocity. The effect of gas content on C_D is

taken into account by modifying the liquid viscosity as $\mu_m = \mu_c / \varepsilon_d$ in the evaluation of the Reynolds number and by multiplying the second part of Equation 10 with

$$f = \left\{ \frac{1 + 17.67\varepsilon_c^{9/7}}{18.67\varepsilon_c^{3/2}} \right\}^2 \tag{12}$$

Additional resistance due to a bubble is caused by the relative acceleration of the bubble in the liquid. This is the added mass force given by Equation 7. Generally the virtual mass coefficient C_{vm} is a function of the volume fraction of the gas phase ε_d with a leading term of value 1. It may also depend on the mass density ratio of the continuous and dispersed phase, i.e. ρ_d / ρ_c, as recently proposed by Zhang and Prosperetti (1996). Zuber's (1964) well-known results for C_{vm} is

$$C_{vm} = \frac{1 + 2\varepsilon_d}{1 - \varepsilon_d} \tag{13}$$

Wijingaaden (1976) and Biesheuvel and Spoelstra (1989) calculated C_{vm} in the dilute limit and found respectively,

$$C_{vm} = 1 + 2.76\varepsilon_d + O(\varepsilon_d^2) \tag{14a}$$

$$C_{vm} = 1 + 3.32\varepsilon_d + O(\varepsilon_d^2) \tag{14b}$$

The difference is due to the different velocity distribution assumed in the calculation. For the cases being considered in the present study where the gas holdup does not exceed 10%, we expect the above first-order expressions to provide a give good approximation, and we choose to use the one by Biesheuvel and Spoelstra (1989), given by Equation (14b).

To predict momentum transfer in bubbly flow it is important to elucidate turbulence of the continuous liquid phase, which may result due to the presence of bubbles. As proposed by Sato and Sekoguchi (1975) the turbulent stress in the liquid phase of bubbly flow can be subdivided into two components, one due to the inherent, i.e. shear-induced, turbulence which is independent of the relative motion of bubbles and the other due to the additional turbulence caused by bubble agitation, i.e. bubble-induced turbulence. Experimental evidence (see Lance and Bataille (1991), and Theofanous and Sullivian (1984)) show that for low holdup bubbly flow the two parts are only weakly coupled so that a linear superposition can be applied. As mentioned before we only model the bubble-induced turbulence.

$$\sigma_c^b = -\rho_c \overline{\mathbf{u}_c' \mathbf{u}_c'} \tag{15}$$

By applying the eddy viscosity model, Sato *et al*. (1981) suggested,

$$\boldsymbol{\sigma}_c^b = \rho_c \eta_b^t \left(\nabla \mathbf{u}_c + \nabla \mathbf{u}_c^{\mathsf{T}} \right) \tag{16}$$

and

$$\eta_b^t = k_b \varepsilon_d d_p \left| \mathbf{u}_c - \mathbf{u}_d \right| \tag{17}$$

where k_b is an empirical constant which usually takes a value of 1.2. This model for the bubble-induced enhancement in viscosity is based on the concept of mixing length, where the bubble radius is taken to be the bubble-induced turbulence length scale.

7.3. Numerical Details

A package, CFDLIB, developed by the Los Alamos National Laboratory (see Kashiwa and Rauenzahn (1994)), is used for the simulations presented in this work. CFDLIB is a hydrocode library for multiphase flow simulations. It uses a cell-centered finite-volume method applied to the time-dependent equations of conservation. Some parts of the code related to the interphase momentum exchange and turbulence calculations are modified according to the models discussed in the last section.

Figure 7.1 shows the mesh system used for the 15-cm wide column. The grid sizes in horizontal and vertical direction are 0.5 cm and 0.8 cm, respectively. In order to obtain a better comparison with experimental data, we set the conditions for our simulations as close to those in Mudde *et al.*'s (1997) experiment as possible. The flow conditions and column sizes for each run are listed in Table 7-1. The gas injectors are numerically realized by setting openings at the bottom of the column which allow only the gas phase passing through at a velocity that, together with gas holdup, matches the value of the gas superficial velocity used in the experiment. Since the size of gas injectors used in the experiments (e.g., 0.16 cm in diameter) is too small to be resolved in the numerical simulation with the currently employed mesh, the openings are about 2 to 4 times larger than the real injectors. It should be noted that in Figure 7.1 the grid is finer at the locations of the gas injectors.

All simulations start from a static initial condition where the main body of the column is filled with water and the top part only with gas. The simulations are then performed until a quasi-steady state is reached. The time-averaged quantities are then calculated as defined in the following expressions,

$$\bar{u}(x) = \frac{1}{N_t} \sum_{n=1}^{n=N_t} u_n(x); \qquad \bar{v}(x) = \frac{1}{N_t} \sum_{n=1}^{n=N_t} v_n(x) \tag{18}$$

$$\overline{u'u'} = \frac{1}{N_t} \sum_{n=1}^{n=N_t} u_n^2 - \bar{u}^2; \qquad \overline{v'v'} = \frac{1}{N_t} \sum_{n=1}^{n=N_t} v_n^2 - \bar{v}^2; \qquad \overline{u'v'} = \frac{1}{N_t} \sum_{n=1}^{n=N_t} (u_n - \bar{u})(v_n - \bar{v}) \tag{19}$$

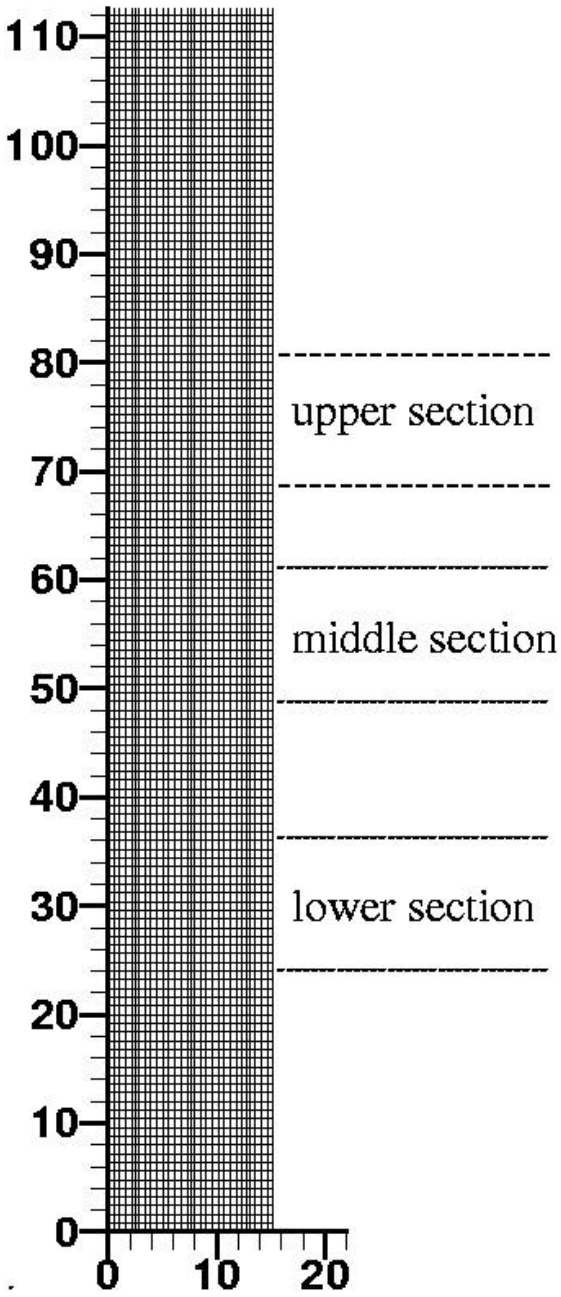

Figure 7.1: Computational Mesh Used For the Simulations of 2-D Column With Discrete Gas Injectors

where $u_n(x)$ and $v_n(x)$ are the horizontal and vertical components of the liquid velocity at time step n. In all simulations the velocity and gas holdup fields are sampled every 0.1 second. To ensure the convergence of the averaged quantities the averaging processes are performed for 50 to 100 seconds which corresponds to a period of time during which about 10 to 20 meandering waves pass through a point at the center-line of the column. The spatial averaging is then performed along the vertical direction within the lower, middle and upper sections as shown in Figure 7.1, respectively. The locations and sizes of these three sections are exactly as same as in Mudde *et al.*'s (1997) experiment.

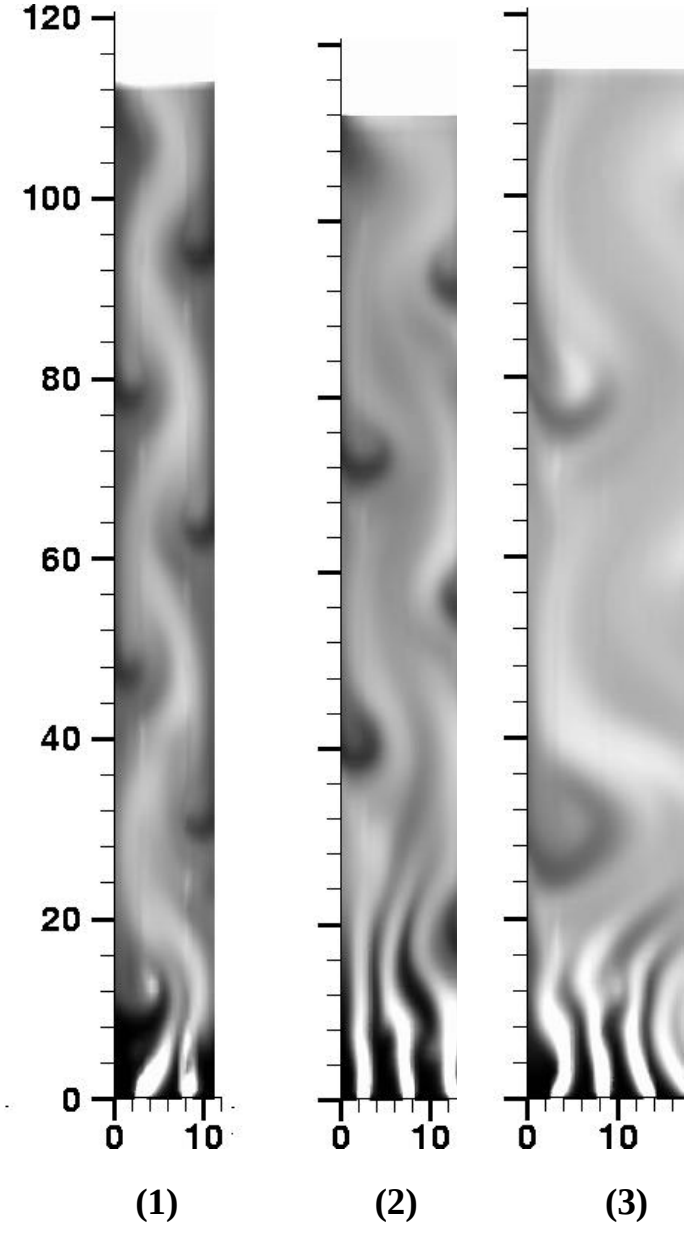

Figure 7.2: Instantaneous Contour Plots for Gas Holdup in (1) 11.2-cm Wide Column at U_{sup}=1 (Cm/s); (2) 15.2-cm Wide Column at U_{sup}= 1 (Cm/s); and (3) 32-cm Wide Column at U_{sup}= 1.2 (Cm/s)

7.4. Large Structures in Bubble Columns

Chen *et al.* (1989) have observed, in their visual study of two-dimensional bubble columns, that when the liquid depth exceeds the column width, i.e. when column's aspect ratio exceeds one, a central wave-like plume accompanied with two staggered rows of vortices which resemble the Karman vortex street appear. Tzeng *et al.* (1993) and Lin *et al.* (1996) further classified the large flow structures in 2-D bubble columns into four distinct flow regions, namely central plume region, fast bubble flow region, vortical flow region and descending flow region. Figure 7.2 shows a snapshot of the instantaneous flow patterns in three columns with different width at the same gas superficial velocity. The central plume with relatively high gas holdup and the vortices adjacent to the side walls are clearly visible. To study the dynamic properties of these large structures we have performed the animations of the flow field by using the velocities and gas holdup generated from the simulations. These animations show that the bubbles injected at the bottom cluster together to move upward in a wavy-like manner while the vortex pairs drift down. The multiple vortex cells that are continually generated in the vortical flow region become confined by the wave motion of central plume. The behavior of these vortices is dynamic in nature, and the formation of these vortices at each side wall appears to be independent of each other. The entire vortex region is swinging laterally back and forth corresponding to the wave motion of the central plume. The structures can be further examined by enlarging the view of a portion of the column. Figure 7.3 shows a snapshot of the liquid velocity vector, liquid vorticity contour and gas holdup contour in a 15-cm wide column. The velocity vectors and vorticity contours clearly indicate the counter-rotating vortex pairs along the side walls.

The dynamic behavior of the large structures is characterized by the wave length and frequency of the meandering central plume. It is expected that these quantities vary with column size and gas (superficial) velocity. Lin *et al.* (1996) have conducted an extensive and detailed experimental investigation, in 2-D columns, on this topic. They have found that, in the same column, the frequency increases with gas velocity while the wave length decreases. At the same gas superficial velocity the frequency decreases as the size (width) of the column increases. The wave-length is proportional to the column size. When the wave length and frequency are multiplied to give the vortex descending velocity, they found that it is basically a function of the gas velocity only. They also found that the size of these vortices is independent of gas velocity and varies with column size only. Figure 7.4 shows the flow pattern in a 15-cm wide column under three different gas velocities. As consistent with the experimental observation, wave length decreases and the overall gas holdup increases as the gas velocity increases. If one performs the spatial fourier transform of the liquid velocity, the wave-length should corresponds to the peak of the power spectra. In figure 7.5 the spatial power spectra of the horizontal component of the liquid velocity field for the three cases depicted in Figure 7.4 are shown. They are calculated by conducting the fourier transform of u along the center line of the column. This value is then averaged over time. As the gas velocity increases, the shifting of the peak towards a larger waver number clearly indicates the shortening of the wave-length. The calculated primary wave-length is 50 cm, 32 cm and 25 cm for U_{sup} =0.25, 1.0 and 2.0 (cm/s), respectively. The measured values, as shown in the figure 8 of Lin *et al.*'s paper, are 25 cm and 21 cm for U_{sup} =1.0 and 2.0 cm, respectively. The difference between the calculated and measured values may partially be due to the fact that the wave length is measured visually in the experiment while it is obtained from the power spectra

in the simulation. Also the smallest variation in wave-length is limited by the spatial resolution used in the simulation. Nonetheless the general trend is certainly captured and consistent with the experimental observations. To study the flow structure in time/frequency domain, we record a time series of liquid velocity at the central point of the column. Figure 7.6 shows such a sample. The meandering motion of the central plume is clearly demonstrated, that is, periods of positive and negative horizontal velocity component alternate. It is interesting to note that while the horizontal motion is dominated by a primary frequency, the vertical motion seems to contain several comparable frequencies. Figure 7.7 shows the temporal power spectra of both u and v at the center line of the column. They are calculated by averaging the spectra at all points on the center line within a middle section of a 15-cm wide column. For the horizontal x-component of liquid velocity the second peak is two order of magnitude smaller than the first one. On the other hand, two comparable peaks appear in the spectra of the vertical y-component of liquid velocity. It should be noted that turbulence is present in both components. Again the calculated primary period is 6.4 seconds while the measured one is 4.4 second as shown in figure 9 of Lin *et al.* (1996).

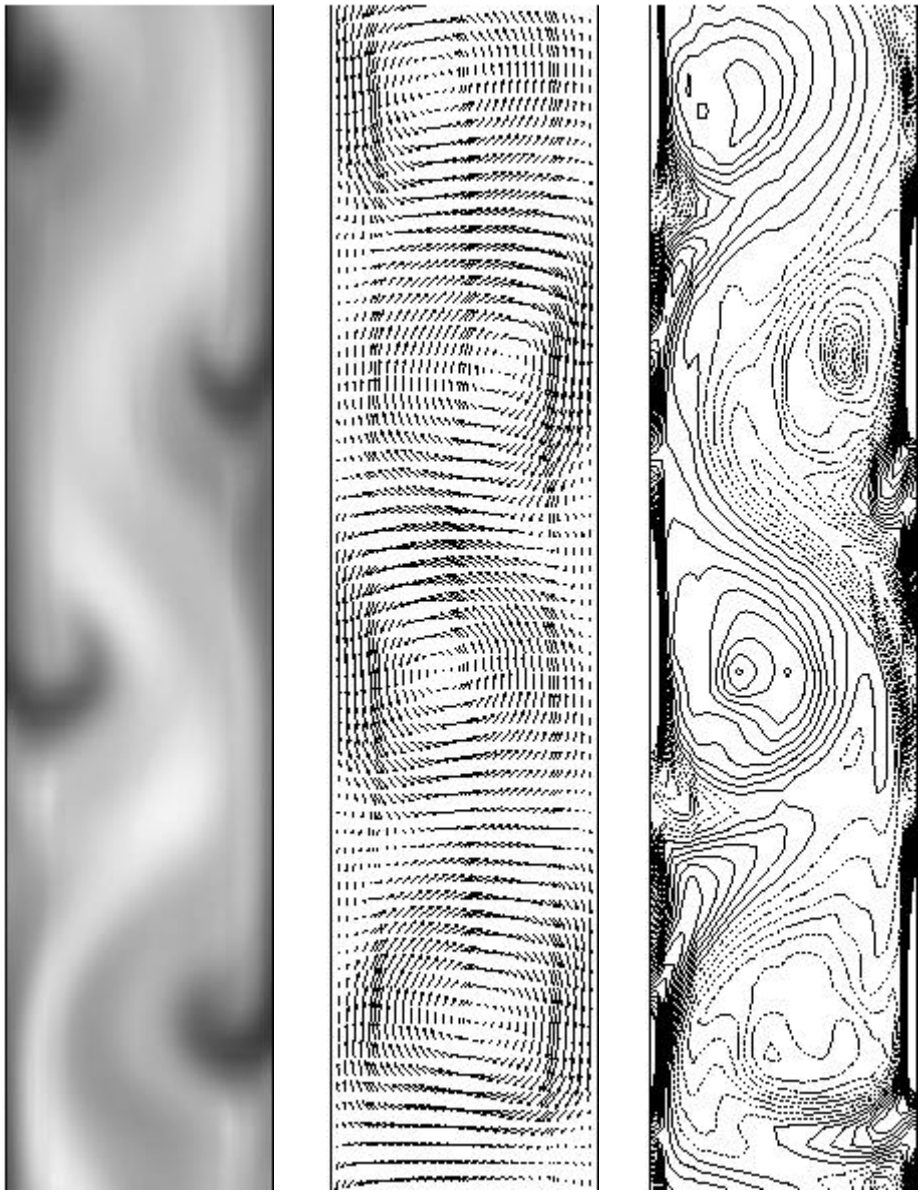

(1) **(2)** **(3)**

Figure 7.3: The Instantaneous Flow Field in a 15-cm Wide Column at U_{sup}=1 (cm/s). (1) Gas Holdup Contour; (2) Liquid Velocity Vector; (3) Liquid Vorticity Contour

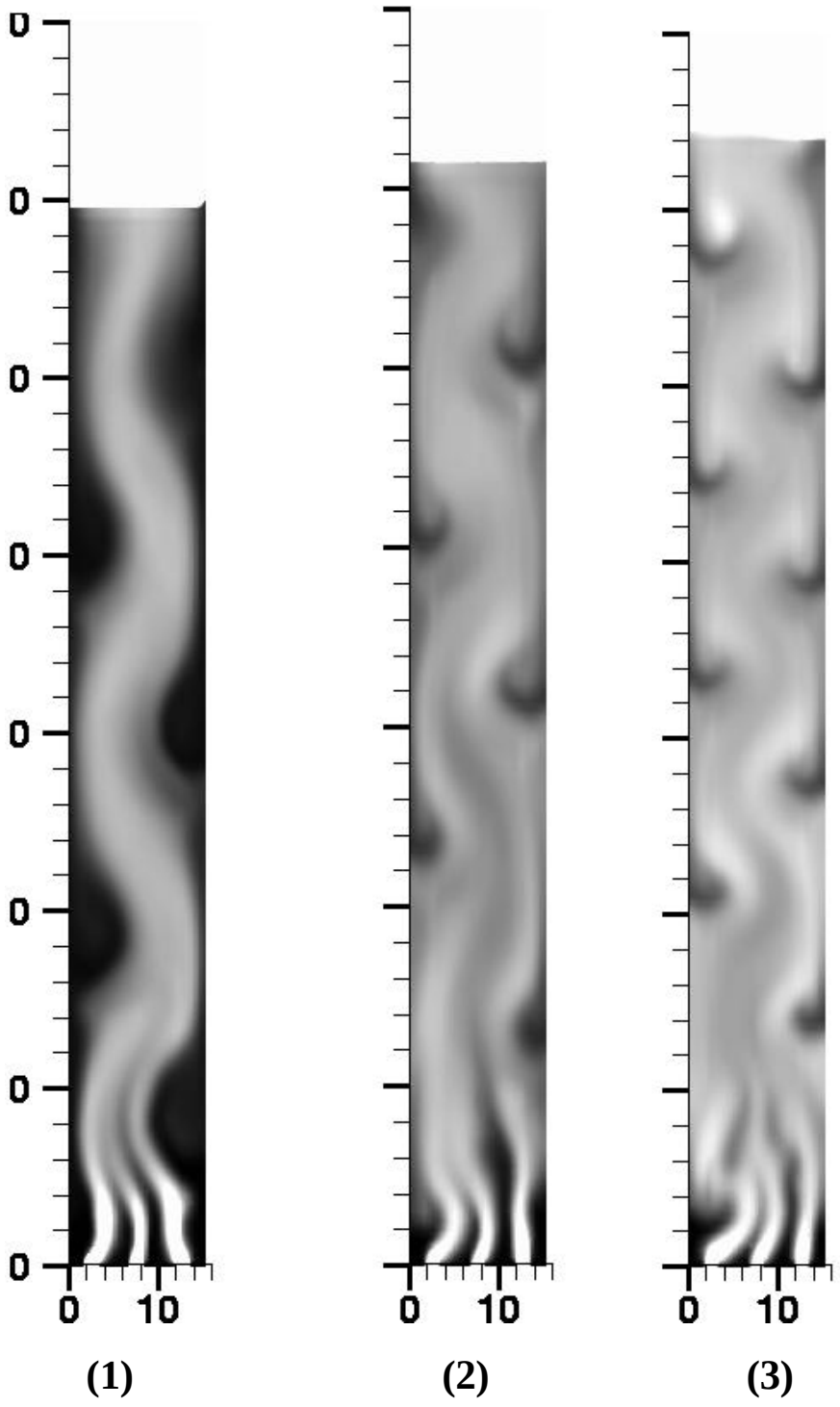

Figure 7.4: Instantaneous Gas Holdup Contours in a 15.2 cm Wide Column Operated at (1) U_{sup}=0.25 cm/s; (2) U_{sup}=1 cm/s; (3) U_{sup}=2 cm/s

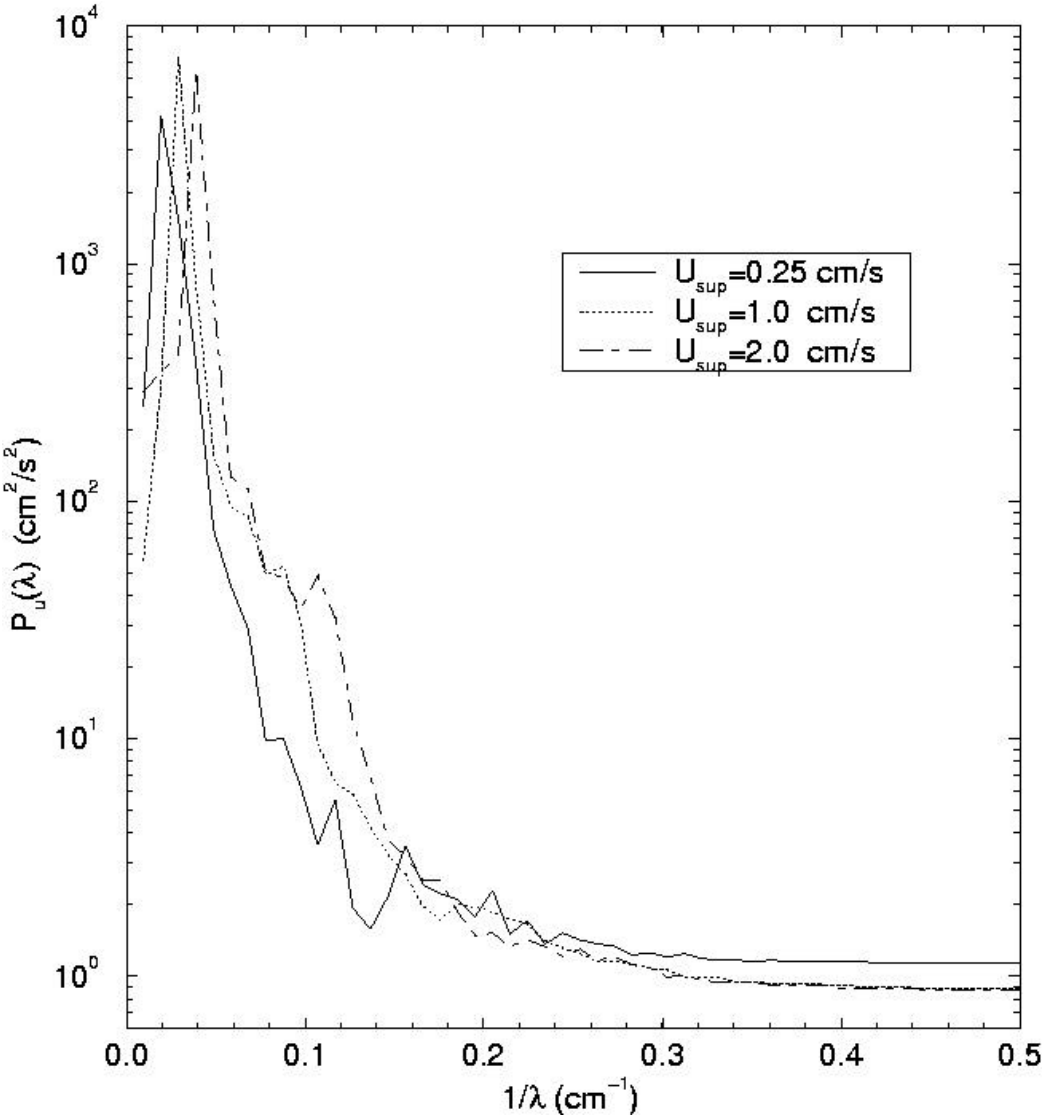

Figure 7.5: Spatial Power Spectra of u in a 15-cm Wide Column at Three Different Superficial Gas Velocities

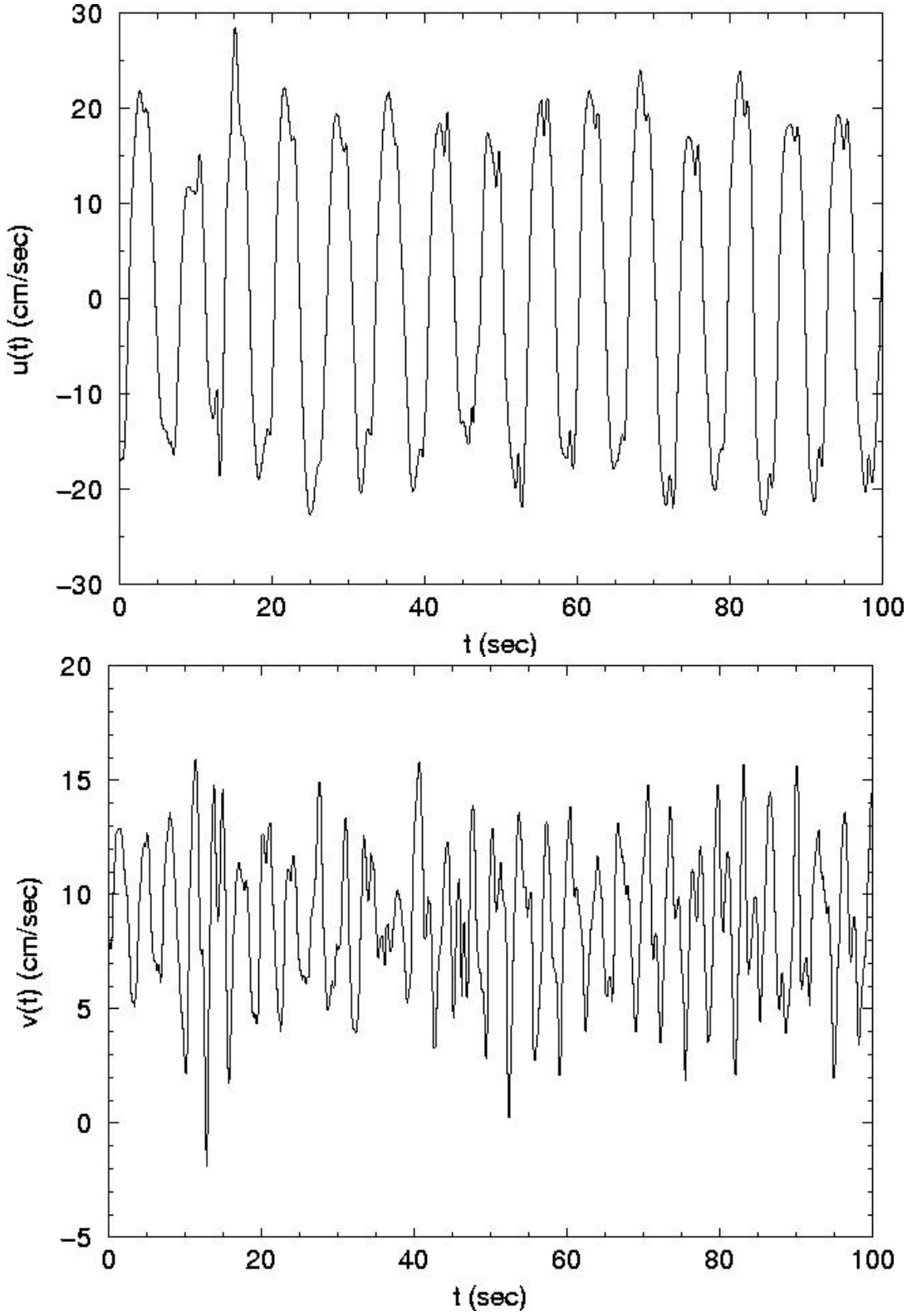

Figure 7.6: Time Series of the Liquid Velocity at the Central Point of 15-cm Wide Column at U_{sup}=1 cm/s

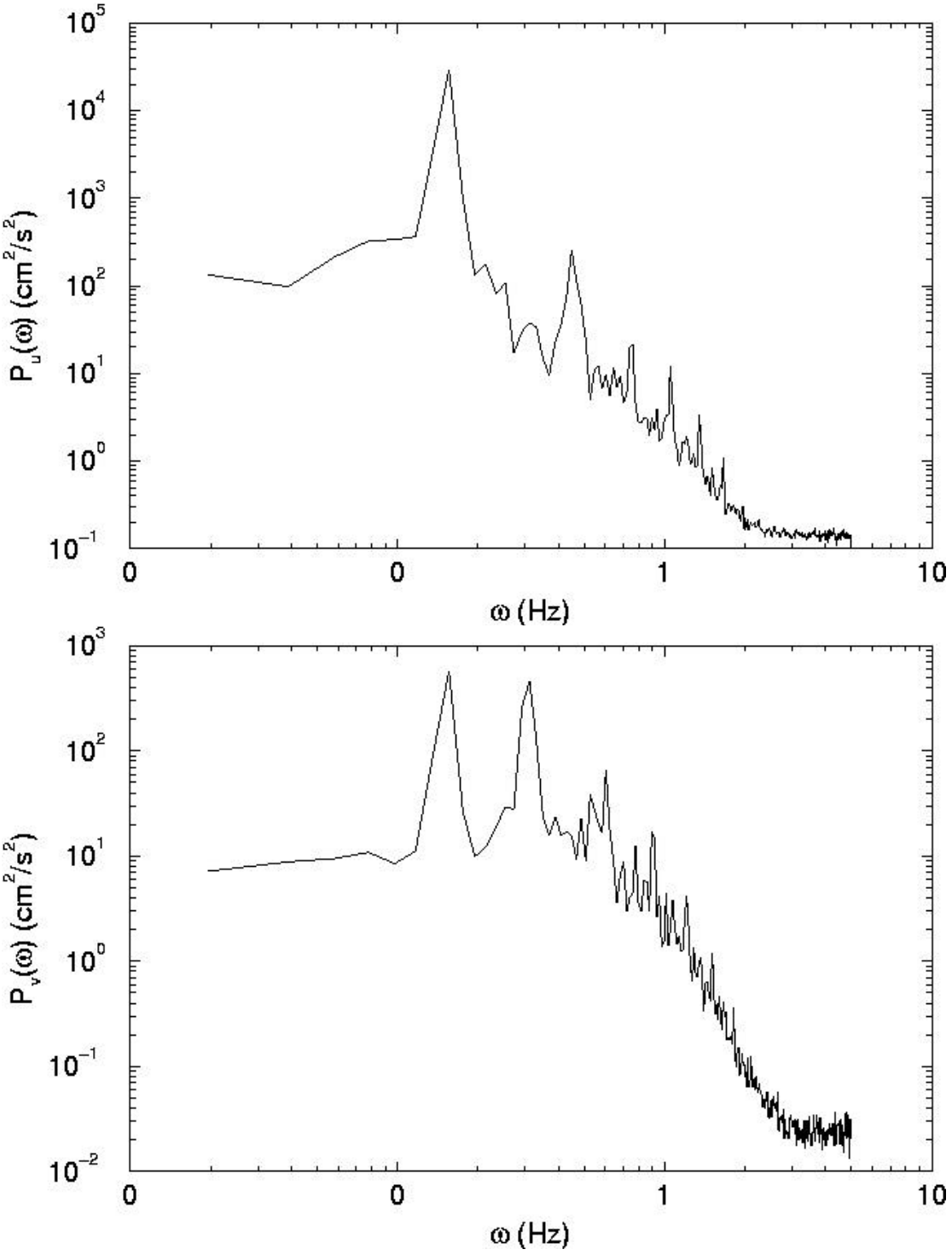

Figure 7.7: Temporal Power Spectra of the Liquid Velocity in a 15-cm Wide Column at U_{sup}=1 cm/s